ELSEVIER

Journal of Alloys and Compounds 446–447 (2007) 19–22

Journal of ALLOYS AND COMPOUNDS

www.elsevier.com/locate/jallcom

Structure of amorphous $CeFe_2D_{3.9}$ observed by X-ray and neutron diffraction

Keiji Itoh [a,*], Kiyoshi Aoki [b], Masaaki Sugiyama [a], Kazuhiro Mori [a], Toshiharu Fukunaga [a]

[a] *Research Reactor Institute, Kyoto University, Kumatori-cho, Sennan-gun, Osaka 590-0494, Japan*
[b] *Kitami Institute of Technology, Koencho-165, Kitami, Hokkaido 090–8507, Japan*

Received 15 September 2006; received in revised form 27 November 2006; accepted 1 December 2006
Available online 5 January 2007

Abstract

X-ray and neutron diffraction measurements have been performed on amorphous (*a*-)$CeFe_2D_{3.9}$ prepared by deuterium absorption of the C15 Laves phase compound $CeFe_2$. Comparison of previous results for amorphous (*a*-)$TbFe_2D_{3.9}$ indicates differences in the location of deuterium atoms. A three-dimensional structural model is proposed for *a*-$CeFe_2D_{3.9}$ on the basis of reverse Monte Carlo (RMC) simulation with X-ray and neutron data. Marked differences in the location of deuterium atoms were found between *a*-$TbFe_2D_{3.9}$ and *a*-$CeFe_2D_{3.9}$.

Keywords: Amorphous materials; Amorphization; Atomic scale structure; X-ray diffraction; Neutron diffraction

1. Introduction

Hydrogen-induced amorphization (HIA), that is, the transformation from a crystalline to an amorphous phase by hydrogen absorption, has been observed in a large number of intermetallic compounds [1]. Although many investigations have been performed to confirm HIA [2,3], the mechanism of this process remains poorly understood [3–5]. To obtain a more complete understanding of the mechanism of HIA, detailed information on the atomic rearrangement induced by hydrogen absorption is required, particularly with respect to the location of hydrogen atoms.

Recently, the present authors studied the structures of *a*-$TbFe_2D_{3.0}$ and *a*-$HoFe_2D_{3.0}$ through reverse Monte Carlo (RMC) simulation using X-ray and neutron diffraction data [6]. It was thus revealed that these two compounds exhibit slight structural differences in the location of deuterium atoms at tetrahedral sites consisting predominantly of rare-earth metal atoms.

Aoki et al. studied HIA for $CeFe_2$ and $TbFe_2$ by pressure-differential scanning calorimetry under a hydrogen atmosphere [7]. It was shown that the process of HIA in $CeFe_2$ differs considerably from that in $TbFe_2$ in that $TbFe_2$ absorbs hydrogen in the crystalline state and subsequently transforms to the amorphous state with increasing temperature, whereas hydrogen absorption and amorphization occur simultaneously and no crystalline hydride *c*-$CeFe_2H_x$ is formed in $CeFe_2$. It is therefore of interest to compare the structure of *a*-$CeFe_2D_x$ with that of *a*-$TbFe_2D_{3.0}$. In this work, the structure of *a*-$CeFe_2D_x$ is investigated by a combination of X-ray and neutron diffraction measurements and RMC modeling, and the results are compared with those obtained previously for *a*-$TbFe_2D_{3.0}$.

X-ray diffraction analysis is advantageous for observing the arrangement of metal atoms in intermetallic compounds due to the large scattering factor for metal atoms compared to deuterium atoms. Conversely, neutron diffraction analysis is a powerful structural probe for locating deuterium atoms, as the coherent neutron scattering length of deuterium is comparable to that of metal atoms. Hence, the combination of X-ray and neutron diffraction measurements provides a means for obtaining comprehensive experimental information on the structure of metal–deuterium systems.

2. Experimental

2.1. Sample preparation

The $CeFe_2$ mother alloy was prepared by arc melting in a purified Ar atmosphere from Ce (99.9% purity) and Fe (99.9%). The ingot of $CeFe_2$ thus

* Corresponding author. Tel.: +81 72 451 2423; fax: +81 72 451 2635.
E-mail address: kgito@rri.kyoto-u.ac.jp (K. Itoh).

0925-8388/$ – see front matter © 2006 Elsevier B.V. All rights reserved.
doi:10.1016/j.jallcom.2006.12.010

obtained was homogenized in an evacuated quartz tube for 605 ks at 973 K to afford a single phase. The crystalline sample was pulverized and activated at 673 K for 3.6 ks, then cooled to 373 K and reacted with high-purity deuterium (99.999%) for 86 ks at a pressure of 0.9 MPa. The ratio of D to metal content in the amorphous sample was determined by the Center for Organic Elemental Microanalysis, Kyoto University to be $CeFe_2D_{3.9}$.

2.2. Neutron and X-ray diffraction measurements

X-ray diffraction measurement was carried out using a horizontal two-axis diffractometer with a photon energy of 113.7 keV (0.01090 nm) at the BL04B2 beam line of the SPring-8 synchrotron radiation facility. The scattering intensity was converted to the total structure factor, $S(Q)$, after corrections for polarization, absorption [8] and Compton scattering [9].

The neutron diffraction measurement was carried out using a high-intensity total scattering spectrometer (HIT-II spectrometer) installed at the pulsed neutron source of the High Energy Accelerator Research Organization (KEK, Tsukuba, Japan). $S(Q)$ was obtained from the scattering intensity after correction for background, absorption [10] and multiple scattering [11], and normalization with a vanadium rod.

The pair distribution functions, $g(r)$, are derived from the Fourier transformation of $S(Q)$ by

$$g(r) = 1 + \frac{1}{2\pi^2 r\rho}\int_0^\infty Q(S(Q)-1)\sin Q\, r\, \mathrm{d}Q \quad (1)$$

where ρ is the average number density of atoms measured using a gas pycnometer (Accupyc 1330, Micromeritics) under 99.999% He gas at room temperature.

The factor $g(r)$ for a ternary mixture can be obtained as a weighted sum of six partial correlations according to the Faber–Ziman definition [12]:

$$g(r) = w_{i-j}\sum_{i,j} g_{i-j}(r) \quad (2)$$

Here, w_{i-j} is the weighting factor defined as

$$w_{i-j} = \frac{c_i c_j b_i b_j}{\langle b\rangle^2} \quad (3)$$

where

$$\langle b\rangle = \sum_i c_i b_i \quad (4)$$

Here, c_i is the concentration and b_i is the coherent scattering length for neutron diffraction or atomic scattering factor for X-ray diffraction, both defined for component atoms i.

RMC simulation [13] was carried out by fitting the model to both X-ray and neutron diffraction data. The starting configurations involved 4000 atoms of appropriate composition distributed randomly in a cubic volume with periodic boundary conditions. Atoms are randomly moved so as to minimize the sum of χ^2 values for respective data sets, where χ is the difference between the experimental structure factor, $S_{\mathrm{exp}}(Q)$, and calculated one, $S_{\mathrm{cal}}(Q)$;

$$\chi^2 = \sum_i \left[S_{\mathrm{exp}}(Q) - S_{\mathrm{cal}}(Q)\right]^2/\sigma_i^2 \quad (5)$$

where σ is the experimental error. The σ values used in this work were 0.01 for both X-ray and neutron diffraction data sets. To ensure a physically realistic configuration, the minimum allowable distances between atoms were determined from the experimental total distribution functions.

3. Results and discussion

The total structure factor obtained by X-ray diffraction measurement for a-$CeFe_2D_{3.9}$ is compared in Fig. 1 with that for a-$TbFe_2D_{3.0}$ [6]. The similarity between the X-ray $S(Q)$ characteristics for these two samples indicates that the atomic

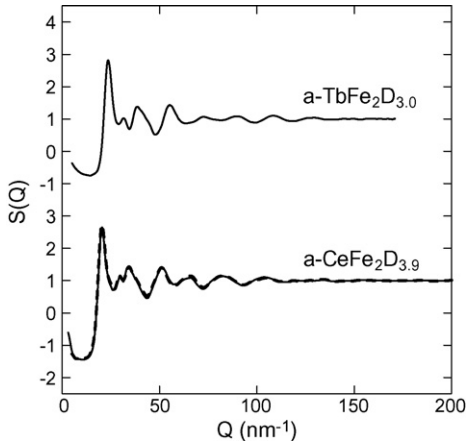

Fig. 1. Total X-ray structure factors, $S(Q)$, for a-$CeFe_2D_{3.9}$ and a-$TbFe_2D_{3.0}$ [6].

arrangement of metal atoms are also similar. It is clear, however, that the peaks in the X-ray $S(Q)$ trace for a-$CeFe_2D_{3.9}$ are located at smaller Q compared to those for a-$TbFe_2D_{3.0}$, reflecting the larger atomic radius of Ce compared to Tb. The neutron $S(Q)$ characteristics are compared in Fig. 2 [6]. The neutron $S(Q)$ traces are also similar, although differences can be seen in the region of small Q. The most notable feature is the presence of a distinct peak at $Q = 0.16$ nm for a-$CeFe_2D_{3.9}$, whereas a-$TbFe_2D_{3.0}$ does not exhibit any clear peak in the region of low Q.

The pair distribution functions for a-$CeFe_2D_{3.9}$ are plotted in Fig. 3. On the basis of the atomic sizes of Fe and Ce atoms, the first three peaks in the X-ray $g(r)$ characteristic can be attributed to Fe–Fe, Fe–Ce, and Ce–Ce correlations. The well-defined first peak in the neutron $g(r)$ trace can be identified as an Fe–D correlation, while the second peak appears to be due to not only Ce–D and D–D correlations but also to Fe–Fe correlations.

The X-ray and neutron total structure factors for a-$CeFe_2D_{3.9}$ obtained by RMC simulation are shown as dashed lines in Figs. 1 and 2. Excellent fitting to both the X-ray and neutron $S(Q)$ traces was obtained. The weighted partial pair correlation functions, $w_{i-j}g_{i-j}(r)$, calculated from the RMC model for a-$CeFe_2D_{3.9}$ are also plotted in Fig. 2, and the coordination

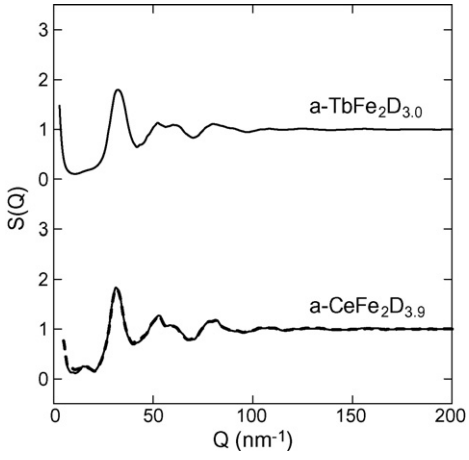

Fig. 2. Total neutron structure factors, $S(Q)$, for a-$CeFe_2D_{3.9}$ and a-$TbFe_2D_{3.0}$ [6].

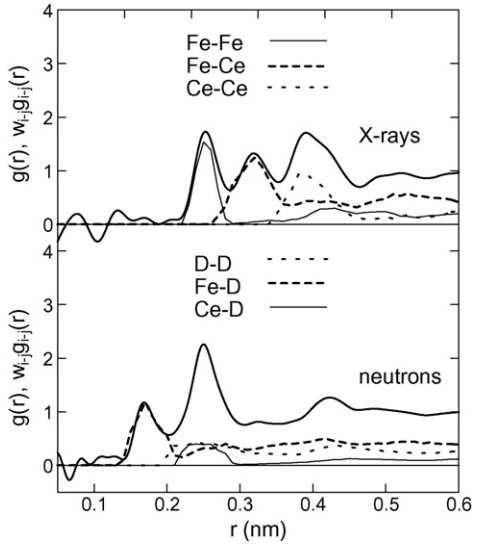

Fig. 3. Total pair distribution functions, $g(r)$, for a-$CeFe_2D_{3.9}$ and weighted partial pair correlation functions, $g_{i-j}(r)$, for Fe—Fe, Fe—Ce, and Ce—Ce (X-ray) and D—D, Fe—D, and Ce—D (neutron) calculated by RMC simulation.

numbers and interatomic distances calculated from the RMC models for both a-$CeFe_2D_{3.9}$ (present data) and a-$TbFe_2D_{3.0}$ (previous data [6]) are summarized in Table 1. The coordination numbers of the like-atom pairs for a-$TbFe_2D_{3.0}$ are larger than for the unlike-atom pairs, indicative of chemical fluctuations of metal atoms. Similar results were also obtained for a-$CeFe_2D_{3.9}$. However, the coordination number of Fe atoms around an Fe atom, $N_{Fe–Fe}$, in a-$CeFe_2D_{3.9}$ is slightly smaller than that for a-$TbFe_2D_{3.0}$, reflecting the larger atomic radius of Ce compared to Tb. Larger $N_{Ce–Ce}$ and smaller $N_{Fe–Ce}$ were obtained by simulation compared to the values calculated on the basis of concentration, suggesting that chemical fluctuation of metal atoms occurs in a-$CeFe_2D_{3.9}$ but to a lesser degree than in a-$TbFe_2D_{3.0}$. The RMC models indicate that most D atoms occupy the tetrahedral sites in both a-$CeFe_2D_{3.9}$ and a-$TbFe_2D_{3.0}$ [6]. However, the conspicuous differences in D site occupancy (Fig. 4) suggest that the D partitioning among the various types of tetrahedral sites differs between a-$TbFe_2D_{3.0}$ and a-$CeFe_2D_{3.9}$. For example, it can be seen that approximately 40% of D atoms occupy 4Tb tetrahedral sites in a-$TbFe_2D_{3.0}$, with D occupancy decreasing in the order 1Fe + 3Tb > 2Fe + 2Tb > 3Fe + 1Tb > 4Fe. These experimental results indicate a strong tendency for Fe and Tb atoms to cluster in a-$TbFe_2D_{3.0}$. On the other hand, approximately 70% of D atoms occupy the 2Fe + 2Ce and 1Fe + 3Ce tetrahedral sites in a-$CeFe_2D_{3.9}$, followed by 20% in 4Ce and 3Fe + 1Ce tetrahedral sites. These results imply that the

Table 1
Nearest-neighbor coordination numbers, N_{i-j}, and interatomic distances, r_1, of metal atoms calculated by RMC simulation

	Fe—Fe		Fe—Ce, Fe—Tb		Ce—Ce, Tb—Tb	
	N_{i-j}	r_1 (nm)	N_{i-j}	r_1 (nm)	N_{i-j}	r_1 (nm)
a-$CeFe_2D_{3.9}$	5.5	0.25	3.0	0.32	6.9	0.39
a-$TbFe_2D_{3.0}$[a]	8.4	0.25	2.4	0.30	7.7	0.36

[a] Values newly calculated from previously reported RMC model [6].

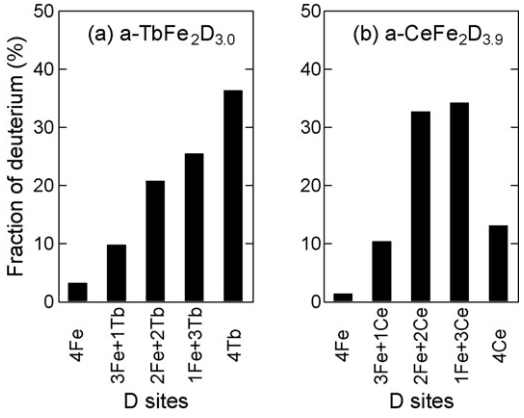

Fig. 4. RMC simulation of D atom partitioning among tetrahedral sites in (a) a-$TbFe_2D_{3.0}$ [6] and (b) a-$CeFe_2D_{3.9}$.

structure of a-$CeFe_2D_{3.9}$ is more homogeneous than that of a-$TbFe_2D_{3.0}$. The present work thus demonstrates that the structure of amorphous hydride prepared by transformation of a crystalline hydride (a-$TbFe_2D_{3.0}$) is more heterogeneous than the structure of an amorphous hydride prepared directly by deuterium absorption (a-$CeFe_2D_{3.9}$).

4. Conclusion

The structure of a-$CeFe_2D_{3.9}$ was investigated by X-ray and neutron diffraction analysis coupled with RMC simulation. The three-dimensional atomic configuration afforded by the RMC simulation reveals differences between the site occupancy of D atoms in a-$TbFe_2D_{3.0}$ and a-$CeFe_2D_{3.9}$. Specifically, D atoms appear to prefer 2Fe + 2Ce and 1Fe + 3Ce tetrahedral sites in a-$CeFe_2D_{3.9}$, and 4Tb and 1Fe + 3Tb sites in a-$TbFe_2D_{3.0}$. Although marked differences in the location of deuterium atoms can be found between a-$TbFe_2D_{3.9}$ and a-$CeFe_2D_{3.9}$, nevertheless structural information of the metal atoms remains in the RMC model. Further investigation of the configuration of the metal atoms will give a full understanding of the mechanism of hydrogen-induced amorphization.

Acknowledgments

This work was supported in part by a Grant-in-Aid for Yong Scientists (B) and a Grant-in-Aid for Scientific Research in Priority Areas A from the Ministry of Education, Culture, Sports, Science, and Technology of Japan.

References

[1] K. Aoki, T. Yamamoto, T. Masumoto, Scripta Metall. 21 (1987) 27–31.
[2] X.G. Li, A. Chiba, K. Aoki, T. Masumoto, Intermetallics 5 (1997) 387–391.
[3] K. Aoki, X.-G. Li, T. Hirata, E. Matsubara, Y. Waseda, T. Masumoto, Acta Metall. Mater. 41 (1993) 1523–1530.
[4] K. Aoki, X.-G. Li, T. Masumoto, Acta Metall. Mater. 40 (1992) 1717–1726.
[5] K. Aoki, T. Yamamoto, Y. Satoh, K. Fukamichi, T. Masumoto, Acta Metall. 35 (1987) 2465–2470.
[6] K. Itoh, Y. Miyajima, K. Aoki, T. Fukunaga, J. Alloys Compd. 376 (2004) 9–16.

[7] K. Aoki, M. Dilixiati, K. Ishikawa, J. Alloys Compd. 356–357 (2003) 664–668.
[8] S. Sasaki, KEK Report 90–16 National Laboratory for High Energy Physics, Japan, 1991.
[9] D. Waasmaier, A. Kirfel, Acta Crystallogr. A 51 (1995) 416–431.
[10] H.H. Paalman, C.J. Pings, J. Appl. Phys. 33 (1965) 2635–2639.
[11] I.A. Blech, B.L. Averbach, Phys. Rev. 137 (1965) 1113–1116.
[12] T.E. Faber, J.M. Ziman, Philos. Mag. 11 (1985) 153.
[13] R.L. McGreevy, L. Pusztai, Molec. Simul. 1 (1988) 359–367.